Int. J. Electrochem. Sci., 16 **(2021)** Article ID: 210314, doi: 10.20964/2021.03.70

International Journal of
ELECTROCHEMICAL
SCIENCE
www.electrochemsci.org

Construction of Fe_3O_4/FeP Binary Composite Catalyst for Degradation of Tetracycline in Wastewater

Huancong Shi[1,], Qiming Wu[1], Xuan Yang[1], Yuanhui Zuo[2,*], Hu Yang[1], Ranran Zhang[1], Yun Zhang[1], Yi Fan[1], Xiaowei Du[4], Linhua Jiang[3,*]*

[1] Department of Environmental Science and Engineering, University of Shanghai for Science and Technology, Shanghai, 200093.
[2] College of Environmental Science and Engineering, Tongji University, Shanghai 200092, China.
[3] Engineering Research Center of AI & Robotics, Academy for Engineering & Technology, Fudan University, Shanghai 200433, P.R. China.
[4] College of Environment and resources, Fuzhou University, Fuzhou 350108, China
[*]E-mail: hcshi@usst.edu.cn, zyh06101@163.com, Jianglinhua@fudan.edu.cn.

Received: 19 November 2020 / *Accepted:* 7 January 2021 / *Published:* 31 January 2021

The abuse of antibiotics greatly aggravates water pollution. Tetracycline hydrochloride (TC), has been widely used all over the world as a typical antibiotic. In order to dispose of TC, a series of Fe_3O_4/FeP composite materials were synthesized with the combination of hydrothermal synthesis and partial phosphating annealing method. Meanwhile, the morphology and structural characteristics were investigated using characterization such as diffraction of X-rays (XRD), scanning electron microscope (SEM), transmission electron microscopy (TEM), electro-chemical impedance spectroscopy (EIS) etc. The dark adsorption and photocatalytic activity of Fe_3O_4/FeP were investigated comprehensively to remove the target molecule tetracycline. Results indicated that Fe_3O_4/FeP catalysts have a superior performance on dark adsorption, and good effect of TC degradation. Among synthesized photocatalysts, Fe_3O_4/FeP-6 (molar ratios of Fe:P at 1:6) possessed the optimized performance in adsorption capacity and photodegradation efficiency (88%) comparing to the other ratios. Furthermore, the stability and reusability of Fe_3O_4/FeP-6 ensured the cyclic photocatalysis experiment. This synthesized catalyst has proved its potential application in wastewater treatment.

Keywords: Fe_3O_4/FeP; photodegradation; tetracycline hydrochloride; in-situ partial phosphating.

1. INTRODUCTION

Antibiotics are typical organic pollutants in wastewater known for its good solubility and non-biodegradable properties [1-3]. These chemicals are harmful to human liver and kidney function through

the metabolism of animals and plants [4, 5]. Recently, environmentalists shift their focus to the trace contaminants in wastewater such as tetracycline (TC), which is world-widely abused due to its low cost and availability [6, 7]. Studies reported that tetracycline not only exhibits toxic effects on aquatic organisms, but also affects the pathogenic microorganisms to develop drug resistance [8-10]. Tetracycline pollution for aquatic environment has become a prominent environmental safety issue [11, 12], so that it is important and urgent to deal with TC by photocatalytic degradation. Photocatalysis is regarded as a promising technology to remove residual tetracycline in water environment [13]. This technology is more effective than activated sludge. Photocatalysts produce free radicals under visible lights, and the radicals effectively decompose the organic chemicals in the wastewater with strong oxidization [14, 15]. Based on literature study, numerous semiconductor photocatalysts have been developed. For instance, Liu et al constructed a three-dimensional (3D) hierarchical photocatalyst CDs/MoS_2@H-TiO_2[6], Zhang et al prepared a CdS/SnO_2 heterojunction photocatalyst [16], Guo et al synthesized a Z-scheme FeOOH/FeS_2 composite photocatalyst [17], all these catalysts have been used to degrade tetracycline by its material advantages and exhibited promising degradation efficiency.

Recently, there are increasingly reports about transition metal phosphides (Ni_2P, FeP, CoP, or Cu_3P), which are mostly used in hydrogen production, but rarely in area of tetracycline degradation. [18-22]. Among transition metal phosphates, iron phosphide (FeP) is widely used in photocatalytic reaction due to its appropriate activation energy [23-25]. Iron phosphide was reported as a promising catalyst with good electroconductivity and stability [26-28], while its photocatalytic activity has been underestimated. Ma et al prepared a new catalyst of FeP that can greatly improve the degradation efficiency of methylene blue (MB) [29], which verified that FeP could be a good photocatalyst, which can be applied to degrade tetracycline as a trial.

Considering loss of photocatalysts after several cycles, Fe_3O_4 is conducive to increases recycling rate if introduced into photocatalysts [30, 31]. Fe_3O_4 has a narrow band gap (0.1 eV) with high conductivity, so that it is a good medium to transfer photogenerated carriers [32-34]. Therefore, the separated efficiency of photogenerated carrier of catalyst can be enhanced to a certain extent if certain materials combined with Fe_3O_4. There are several publications about Fe_3O_4-based composite accelerating photocatalytic degradation effect, such as Fe_3O_4/g-C_3N_4 [30], ZnO/Fe_3O_4 [5], TiO_2/Fe_3O_4 [31], the benefits of Fe_3O_4 lies in increased degradation rates and stability of recycle.

Herein, we adopt in-site partial phosphating strategy to construct a new visible-light driven oxidation composite material Fe_3O_4/FeP with simple hydrothermal and thermal annealing processes. By adjusting the molar ratio of FeOOH precursor and NaH_2PO_2 as Fe:P, this study synthesized different photocatalysts of Fe_3O_4/FeP-4~8. The Fe_3O_4/FeP catalysts were characterized with XRD, SEM, TEM, BET, UV-vis diffuse reflection spectroscopy (DRS) and EIS methods. For the dislodge of TC, the adsorption capacity and photocatalytic activity of Fe_3O_4/FeP were studied comprehensively. The cyclic experiments were adopted to prove the stability and reusability of Fe_3O_4/FeP. Since FeP are seldom used in wastewater treatment to degrade tetracycline, this study is an innovative trial to provide an alternative material for the TC degradation in wastewater treatment industry.

2. EXPERIMENT SECTION

2.1. Preparation of Catalysts

Synthesis of FeOOH: 1.44 g of $FeSO_4 \cdot 7H_2O$ and 10-15 mL of glycerol were dissolved in 120 mL deionized water and stirred for 30 min to prepare a uniform solution. Then the solution was transferred into a 150 mL Teflon autoclaves, which was heated in an oven at 110 ℃ for 12 hours. After cooled down to 298K, the samples were centrifuged with pure water and ethanol repeatedly, the precipitate was dried overnight in a 60 ℃ oven to produce FeOOH precursor finally.

Synthesis of Fe_3O_4/FeP: 0.89g of FeOOH and different amounts of NaH_2PO_2 were weighted and placed at two separated position in a closed porcelain crucible, where NaH_2PO_2 was at upstream side of the furnace. It was heated at 350 ℃ for 2 hours with heating rate of 2℃ min^{-1} under the N_2 gas flow. After cooled down to room temperature, the samples were collected with centrifugation and rinsed with distilled water and ethanol repeatedly. The collected samples were dried in an oven at 60 ℃ for 12 hours. The molar ratios of FeOOH to NaH_2PO_2 varied at different ratios (1:4, 1:5, 1:6, 1:7, 1:8) during the synthesis process in preparation for samples. These samples were denoted as Fe_3O_4/FeP-4, Fe_3O_4/FeP-5, Fe_3O_4/FeP-6, Fe_3O_4/FeP-7, Fe_3O_4/FeP-8, respectively.

2.2. characterizations of samples

Diffraction of X-rays (XRD) patterns were observed on a D/MAX-2500 diffractometer (Bruker, German) using a Cu Ka radiation source (λ=1.5418 Å). SEM images were performed using Scanning electron microscope (Hitachi S-4800, Japan). TEM and HRTEM images were utilized Talos F200x (Thermo Fischer, Japan) transmission electron microscopy. The X-ray photoelectron spectroscopy (XPS) was investigated by Thermo Scientific K-Alpha using Al Kα X-ray (hυ=1486.6 eV) electron spectrometer. The UV-vis DRS were performed by using UV2600 (Shimadzu, Japan) diffuse reflectance spectrometer with $BaSO_4$ as a reference, and the scanning range 200-800 nm. The BET specific surface area and pore property were measured by a surface area analyzer (NOVA 2200e, Quantachrome). Electrochemical impedance spectroscopy (EIS) tests were investigated on the CHI660E electrochemical workstation (Chenhua Instruments Co. Shanghai china). The Pt plate and saturated Ag/AgCl electrode were used as auxiliary electrode and reference electrode. The prepared samples Fe_3O_4/FeP-4~6 were served as working electrode, and 0.5M H_2SO_4 was used as electrolyte. The catalyst Fe_3O_4/FeP-6 of 0.02 g, PVDF of 0.16 g and carbon of 0.02 g were dissolved in 1-Methyl-2-pyrrolidone of 500 μL to form homogeneous suspension, which was then coated on copper sheet with the size of 10×20 mm. The detailed operation parameters were set as follow, initial E = 0.055V (FeOOH), and E = 1.231V, 0.728V, 0.035 V(Fe_3O_4/FeP-4~6), High Frequency = 10^{+5} Hz, Low frequency = 1 Hz. Amplitude = 0.005 V. Quiet time = 2 sec.

2.3. Photocatalytic activity experiments

Photodegradation of TC was performed to evaluated the activity of Fe_3O_4/FeP. The photocatalytic experiments were performed under a 1000 W Xenon lamp, and the temperature of reaction

was maintained at 20 ℃. Prepared TC solution (50 mg/L) was treated with ultrasonication for 20 min. 20 mg Fe_3O_4/FeP-4~8 samples were spread into 40 mL TC solution (50 mg/L) for each set of degradation experiments, so that concentration of catalyst is 0.5 g/L. Before illumination, the solution was stirred for 30 min under dark conditions to exclude the influence of strong adsorption onto TC. After then, 3 mL sample were pipetted every 20 min under illumination condition, adding 3 mL distilled water for dilution and centrifuge. The diluted samples were centrifuged twice at a speed of 10000 r/min to remove the precipitation. The whole photodegradation process lasted 3 hours, and the residual concentration of TC of as-prepared samples were detected with a UV-vis spectrophotometer at 360 nm, which was the characteristic wavelength of tetracycline hydrochloride.

3. RESULTS AND DISCUSSION

3.1 Characterization analysis of samples

The morphological features of the as-synthesized samples were investigated by SEM and TEM. The SEM images were shown in Fig. 1a and b, the FeOOH precursor displayed a petaloid hierarchical spheres composed of nanoflakes and nanorods, and the diameter of the spheres were ~1.5 μm. From SEM images of Fig. 1c-d, the surface of Fe_3O_4/FeP-6 microspheres were rough and it consisted of massive finer nanostructures, which was well inherited from FeOOH precursor. The diameter of Fe_3O_4/FeP-6 was a little bigger than that of FeOOH microspheres. The TEM images of Fe_3O_4/FeP-6 plotted in Fig. 1e-g exhibited a petaloid structure, and their surface were discovered to have apparent whiskers with the size of 100 nm to 200 nm. This special structure was beneficial to increase the contact surface area between catalysts and TC molecules. The high-resolution TEM (HRTEM) was utilized to investigate the structure of Fe_3O_4/FeP-6. The HRTEM images of Fig. 1h showed two different interplanar spacings of 0.195 nm and 0.294 nm, which was in correspondence to (121) plane of FeP and (220) plane of Fe_3O_4 [5, 26]. The catalysts Fe_3O_4/FeP was proved by High-Angle Annular Dark Field (HAADF) images of Fig. 1i, along with its corresponding element mapping (EDS) images of Fig. 1j-l. EDS images illustrated that Fe, P and O elements were uniformly distributed over the surface of Fe_3O_4/FeP-6. These results demonstrated that a new catalyst of Fe_3O_4/FeP had been synthesized successfully.

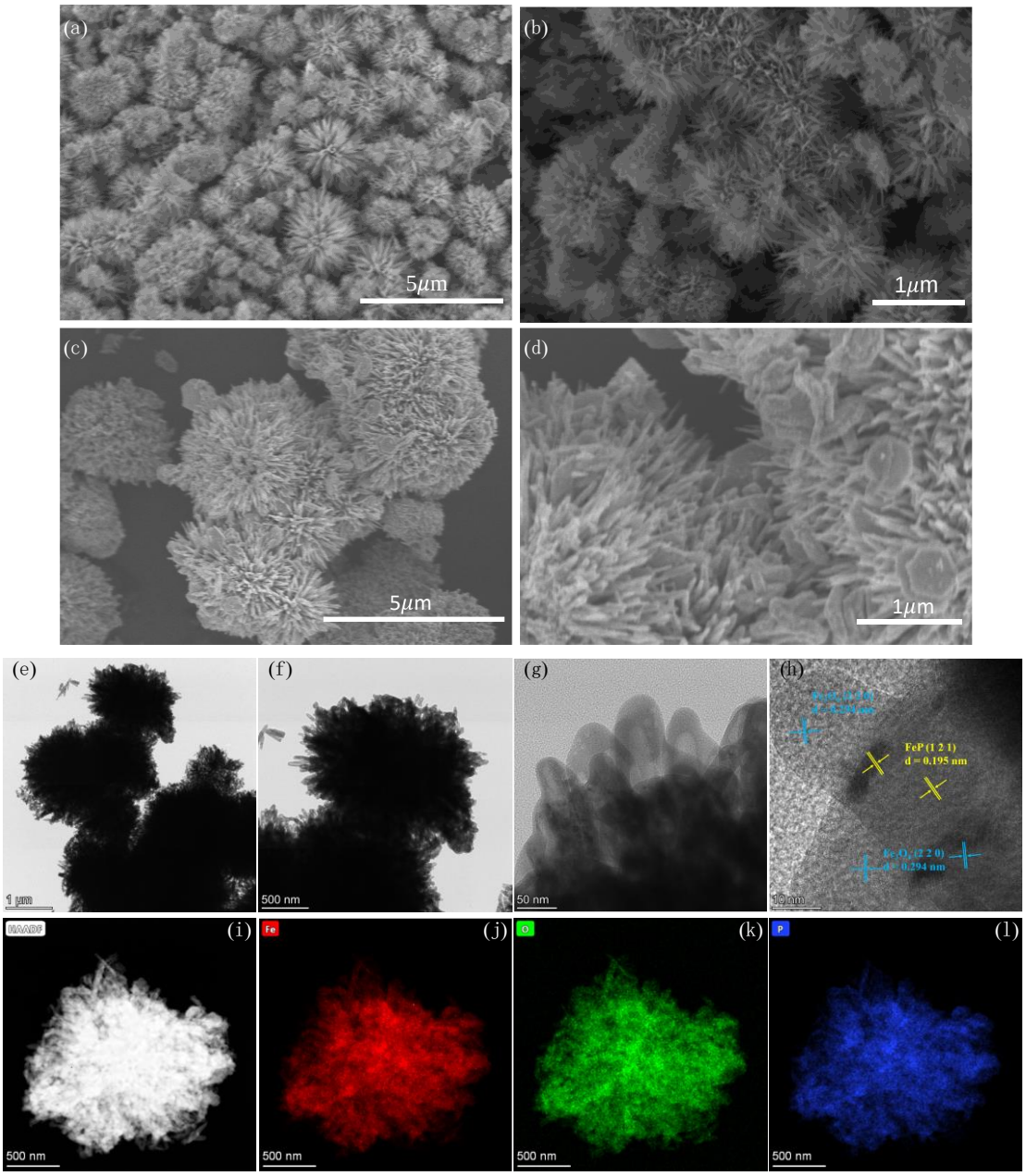

Figure 1. SEM images of FeOOH (a-b), Fe_3O_4/FeP-6 (c-d), TEM images of Fe_3O_4/FeP-6 (e-g), HRTEM images of Fe_3O_4/FeP-6 (h), HAADF image (i) and EDS mapping (j–l) of Fe_3O_4/FeP-6.

XRD were used to detect the crystal structure of as-prepared samples. Fig. 2 showed the XRD patterns of FeOOH precursor and Fe_3O_4/FeP-6. The diffraction peaks of FeOOH precursor were clear and corresponded to JCPDS NO. 29-0713, where distinct diffraction peak at 21.2°, 33.2°, 34.7°, 35.5°, 36.6° and 41.2° is atttributed to (110) (130) (021) (101) (111) (140) lattice planes. The XRD diffraction pattern of Fe_3O_4/FeP-6 indicated the weak diffraction peaks of two components, where diffraction peak were clearly observed at 30.1°, 35.4° and 62.5° corresponding to (220) (311) (440) lattice planes of Fe_3O_4 (JCPDS NO. 19-0629), and the diffraction peak were located at 32.7°, 46.3°, 46.9° and 48.3° in

aggreement with (011) (121) (220) (211) lattice planes of FeP (JCPDS NO. 39-0809). The XRD results confirmed the formation of Fe_3O_4/FeP composite.

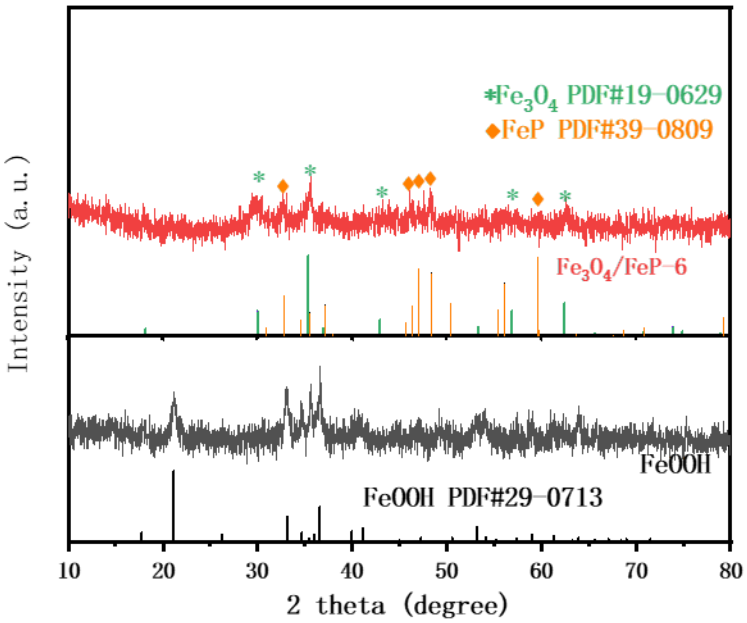

Figure 2. XRD patterns of FeOOH and the composite of Fe_3O_4/FeP-6

XPS characterization of Fe_3O_4/FeP-6 was performed to determine the surface composition and element valence state of as-prepared samples. From Fig. 3a, the XPS spectrum of Fe_3O_4/FeP-6 exhibited element of Fe, P, O and C, which was in connection with the EDS elements mapping results. In addition, the calibration of all elements was based on the binding energy of C (C 1s = 284.8 eV). XPS spectra was displayed in Fig. 3b. The main peaks at 712.1 and 725.9 eV were assigned to Fe $2p_{3/2}$ and Fe $2p_{1/2}$ components, and a satellite peak at 714.1 eV might arise from Fe surface oxidation [26, 35]. A peak around 707.5 eV was the characteristic peak of Fe-P from FeP [27, 36], which was not sharp due to the low content of iron phosphide in the composite of Fe_3O_4/FeP. The peak at the binding energy of 129.1 eV were divided into two peaks 129.3 and 129.9 eV, which is corresponded to P $2p_{3/2}$ and P $2p_{1/2}$ (Fig. 2(c)). The peak around 133.5 eV was assigned to P-O bonding structure of oxide form, which might result from surface oxidation [29]. The O 1s XPS spectra were fitted into four peaks at 530.2, 530.8, 531.6 and 532.8 eV, which was attributed to bonds of Fe-O, -OH, Fe-P-O and C=O [35].

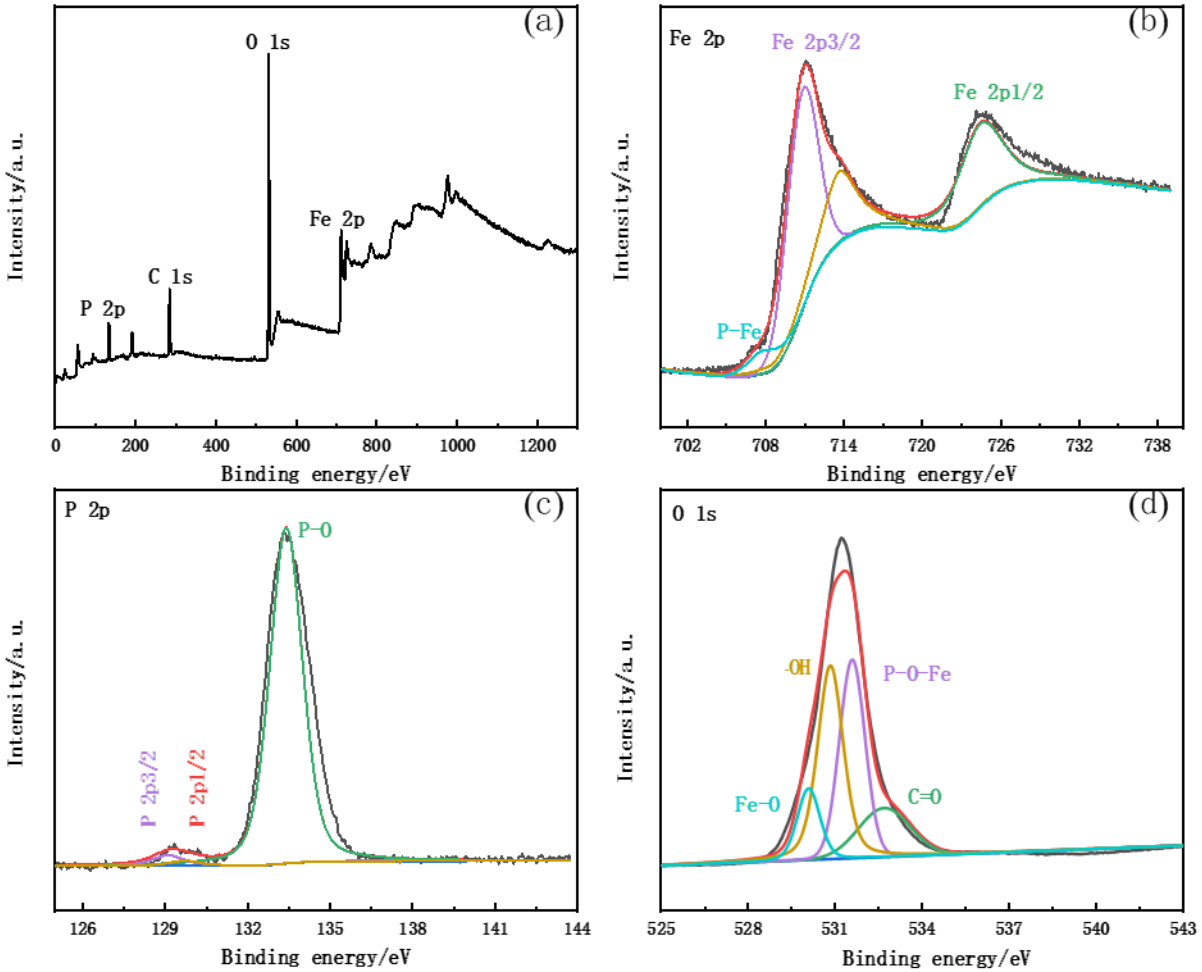

Figure 3. XPS spectra of Fe_3O_4/FeP-6: (a) the full spectrum diagram, (b) Fe 2p, (c) P 2p, (d) O 1s.

UV-vis DRS were adopted to investigate the optical property of prepared samples. Fig. 4 showed the light adsorption intensity curves of the FeOOH and Fe_3O_4/FeP-4~8. The FeOOH precursor exhibited strong adsorption in the ultraviolet wavelength range (200-450 nm), but relatively weak in the visible band (500-800 nm). Results indicated that FeOOH could not adsorb photons of the visible light band to produce enough photogenic carriers, resulting in its low photodegradation efficiency. However, the synthesized catalysts Fe_3O_4/FeP-4, 5, 6, 7, 8 all had adequate light response range and were capable of absorbing enough photons of visible/ultraviolet. The optical adsorption curves of the catalysts were not smooth due to the impurity of composite Fe_3O_4/FeP. The optical adsorption results showed that these Fe_3O_4/FeP-4~8 reflect good response to visible light with intense light absorption ability.

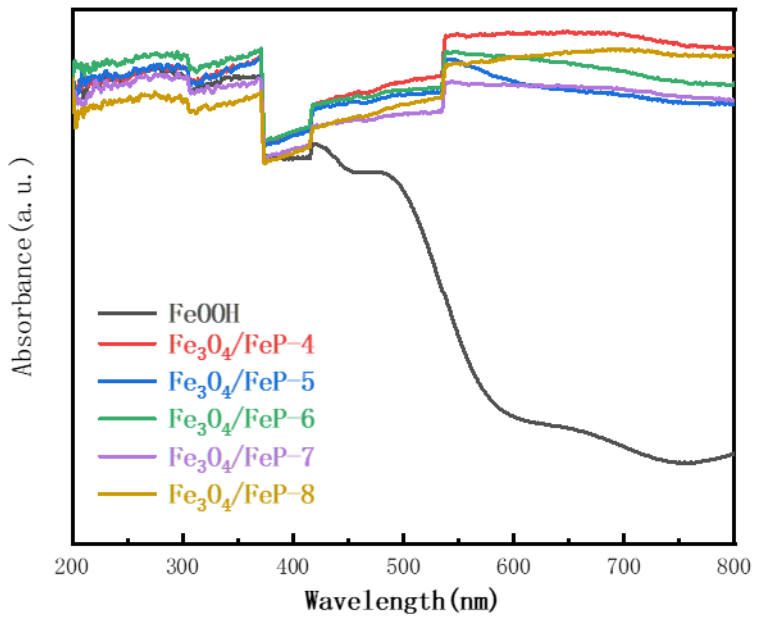

Figure 4. UV–vis DRS of FeOOH and Fe_3O_4/FeP-4, 5, 6, 7, 8.

The N_2 adsorption-desorption experiments were performed to determine the pore size property and BET specific surface area of as-prepared samples. Fig. 5a showed the N_2 adsorption-desorption isotherm of FeOOH precursor and Fe_3O_4/FeP-6. According to the classification standard of IUPAC, the isotherm of FeOOH and Fe_3O_4/FeP-6 displayed a typical type-IV with H_3 hysteresis loop among the relative pressure (p/p_0) range from 0.5 to 1.0, which proved that these catalysts were mesoporous. Fig. 5b showed the pore diameter distributions curve of FeOOH and Fe_3O_4/FeP-6. The pore diameter of FeOOH were distributed around 30 nm, while Fe_3O_4/FeP-6 exhibited the pore diameter distribution from 10-20 nm. The difference might result from the change of morphology of FeOOH after the phosphating process turned it into a smaller pore size in Fe_3O_4/FeP-6. Furthermore, the total pore volume of Fe_3O_4/FeP-6 (0.311 cm^3/g) was 3.42 times than that of FeOOH (0.091 cm^3/g). The large volume resulted in good diffusion effects for TC molecules to active sites. The BET specific surface area was 96.50 m^2/g of Fe_3O_4/FeP-6, which was comparable to the reported value of 90.50 m^2/g. [37] The BET of FeOOH was 21.330 m^2/g, which was much smaller than the urchin-like FeOOH microspheres (120.5 m^2/g) [37] because of different preparation methods and different morphologies.

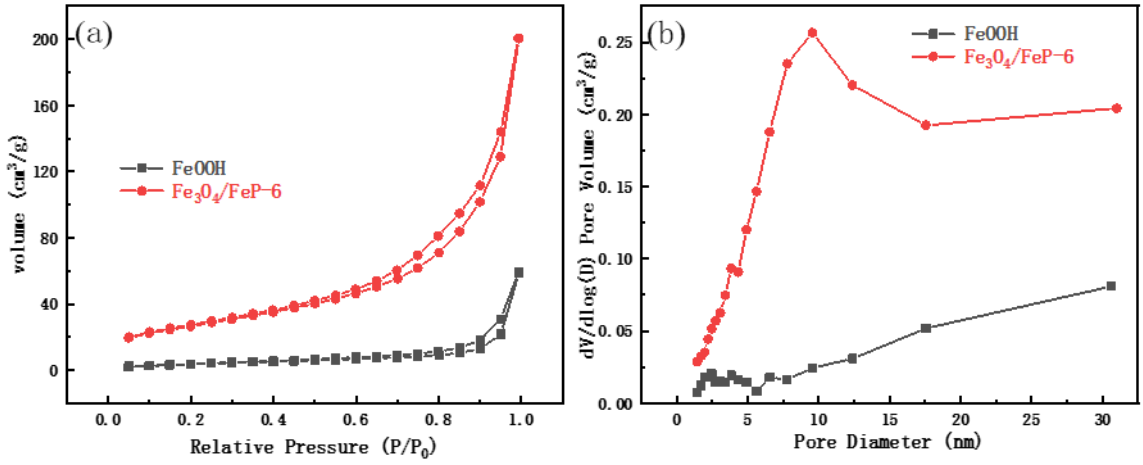

Figure 5. N_2 adsorption-desorption isotherm (a) and pore size distributions of (b) FeOOH and Fe_3O_4/FeP-6.

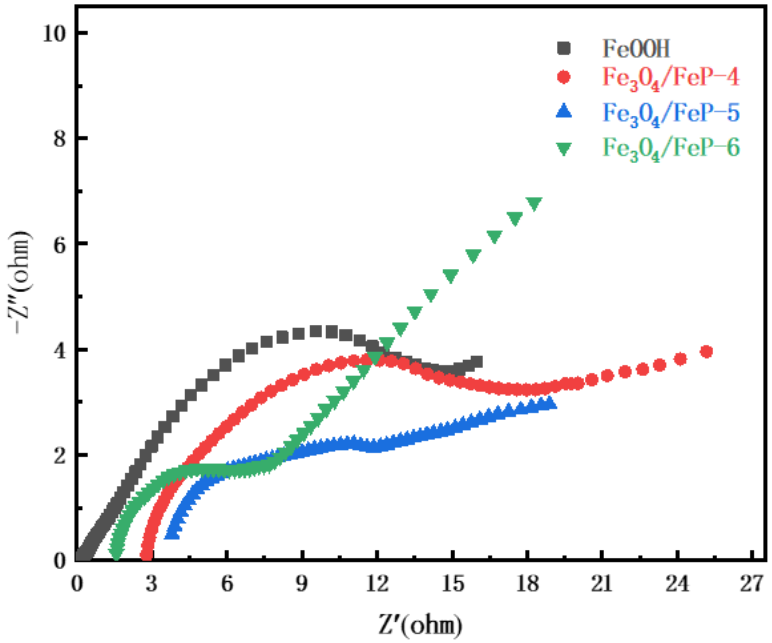

Figure 6. The Nyquist plots of as-synthesized samples: Fe_3O_4/FeP-4, 5, 6, and FeOOH

The charge-transfer procedure of as synthesized samples Fe_3O_4/FeP-4~6 and FeOOH were analyzed through EIS measurement. From Fig. 6, the semicircle was considered as the charge-transfer resistance (Rct) of H^+ reduction at the electrode–electrolyte interface. From Figure 6, the Rct of FeOOH was 18 Ohm, close to literature values ranged from 2-40 Ohm [17,38,39]. The curves indicated that the Nyquist arc radius of both FeOOH and Fe_3O_4/FeP-6 were very small due to good electro conductivity. The charge transfer resistance (Rct) of Fe_3O_4/FeP-4 was 20 ohm, Fe_3O_4/FeP-5 was 16 ohm, and Fe_3O_4/FeP-6 was about 8~10 ohm, with order of Fe_3O_4/FeP-4 > Fe_3O_4/FeP-5 > Fe_3O_4/FeP-6, the smaller the better. These results were comparable to the published EIS plots of FeP catalysts [26, 40, 41]. Li et al reported the Rct of FePNRs (fabricated iron phosphide nanorods) was 11 ohm [40]. Tian et al reported FeP/GR (FeP nanoparticles film with rigid graphite rod) exhibited Rct of 20-22 ohm, and FeP-GS/CC

(FeP nanoparticles film grow on graphene sheet and carbon cloth) with Rct of 30 ohm.[41] Other researchers reported Rct of FeP as 150 ohm, FeP/C (FeP with 20 wt% carbon content) as 300 ohm [26], which were much larger since their FeP was heated to 300 °C during preparation. In summary, as-prepared Fe_3O_4/FeP-6 composites in this study had the smallest Rct value because they contained inpurities of Fe_3O_4, which possessed high electron transfer efficiency and faster interface charge transfer ability.

3.2 Adsorption and photocatalytic activity evaluation

The adsorption and photocatalytic activity of Fe_3O_4/FeP were evaluated on TC degradation experiments. Fig. 7a showed the adsorption curves of TC under dark adsorption over the FeOOH precursor and Fe_3O_4/FeP-4~8 composites. Results indicated that Fe_3O_4/FeP-4~8 all showed superior adsorption capacity compared to FeOOH precursor, which might arise from larger pore volume and the surface area of Fe_3O_4/FeP of this study. These tiny holes facilitated photocatalyst Fe_3O_4/FeP to adsorb more TC molecules. Among Fe_3O_4/FeP catalysts, the adsorption capacity of Fe_3O_4/FeP-4, 5, 6 was surperior to that of Fe_3O_4/FeP-7,8. The Fe_3O_4/FeP-6 catalyst had the best performance within 5 ratios in its adsorption capacity with 58% in 150 min, and the adsorption capacity followed the order of Fe_3O_4/FeP 1:6 > 1:5 > 1:4 > 1:7 > 1:8.

Fig. 7b showed the photodegradation dynamic curves of TC under irradiation of 180 min visible light after 30 min dark adsorption with existence of the FeOOH precursor and Fe_3O_4/FeP-4~8. The degradation efficiency of the FeOOH precursor was only 24%. The degradation efficiency of TC over Fe_3O_4/FeP composites varied with different ratios of Fe:P. With increasing contents of NaH_2PO_2 in the phosphating process, the photodegradation rates of Fe_3O_4/FeP composites reached the optimum of 88% for Fe_3O_4/FeP-6 after 30 min dark adsorption and 180 min illumiantion of visible light. If the molar ratio of Fe:P increased to 1:7 and 1:8, the degradation rate began to decrease markedly, which might result from the disruption of petaloid hierarchica structure of Fe_3O_4/FeP. From the curves of Fig. 7b, the degradation followed the order of 1:6 > 1:5 >1:4 > 1:7 > 1:8, consistent with the order of dark adsorption effect.

Fig. 7c showed the rate constant k value of TC over Fe_3O_4/FeP-4~8 according to the kinetic model of the first order reaction: $\ln(C_0/C) = kt$. The key parameter was were ploted as the rate constant (k) of photocatalysts, and Fe_3O_4/FeP-6 had the largest rate constant k = 0.00984 min^{-1}. The rest k were 0.00864, 0.00884, 0.00694 and 0.00654 min^{-1} for Fe_3O_4/FeP-4, 5, 7, 8. Results indicated that the Fe_3O_4/FeP-6 had the best performance in adsorption capacity and photocatalytic.

In addition, Fig. 7d showed the UV-vis adsorbance spectrum of TC over Fe_3O_4/FeP-6 during photodegradation process. The absorbance of TC decreased distinctly among the wavelength range of 280 to 400 nm under illumination, which indirectly verified that TC were decomposed into small molecules/ions with increased time.

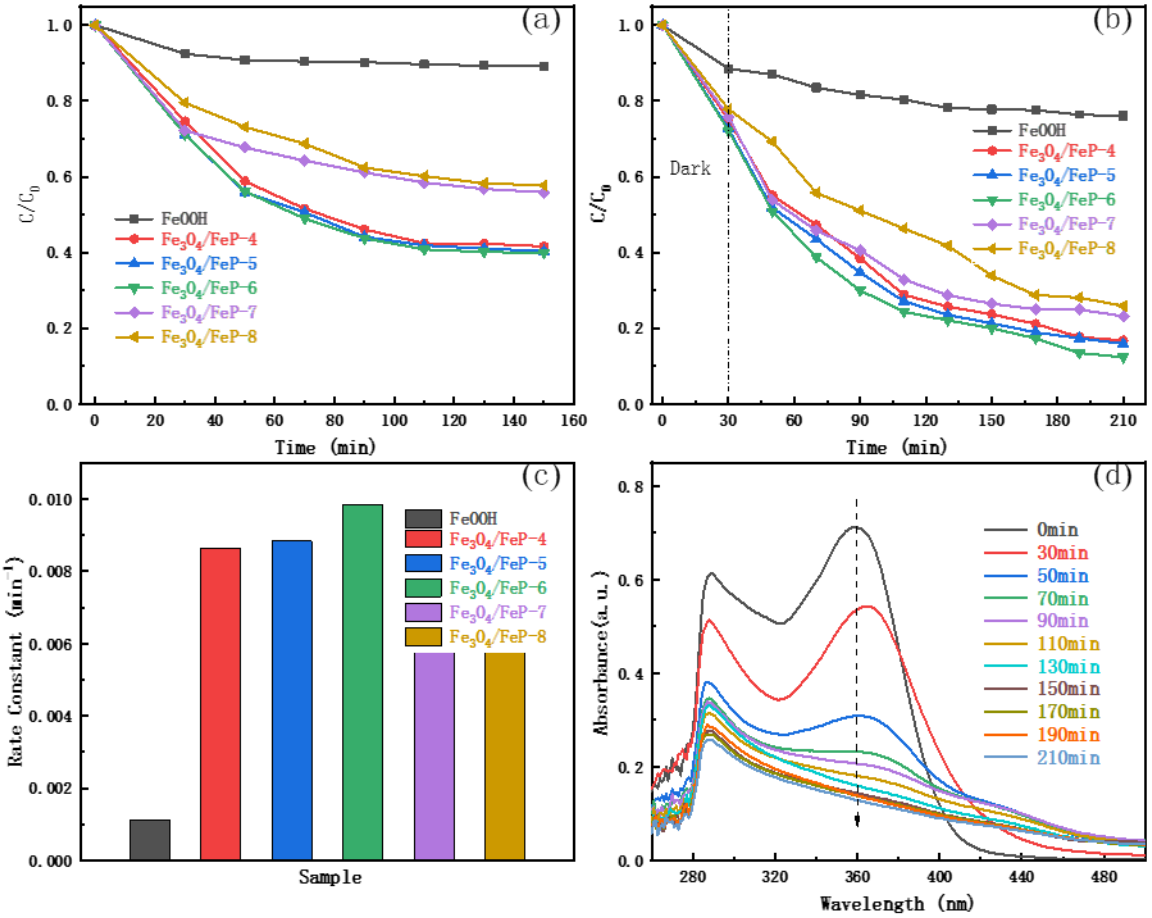

Figure 7. Dark reaction adsorption curve (a), degradation dynamic curves (b), rate constants (c) of TC over FeOOH and Fe_3O_4/FeP-4~8, and absorbance of TC over Fe_3O_4/FeP-6 (d).

Table 1. Photo degradation effects of TC among different catalysts.

Photocatalysts	Catalyst dosage （mg/L）	TC Concentration （mg/L）	W_{cat}/TC (mg/mg)	Dark (min)	Illumination (min)	Removal rate	Reference
FeOOH/FeS_2	500	10	50	30	150	90%	Guo et al. [17]
Ag/Fe_3O_4/g-C_3N_4	500	20	25	50	90	88%	Zhu et al. [42]
$SrTiO_3$/Bi_2O_3	1000	10	100	30	140	85%	Che et al. [9]
CDs/MoS_2@H-TiO_2	500	10	50	40	180	82%	Liu et al. [6]
Sn_3O_4/g-C_3N_4	500	10	50	30	120	72%	Li et al. [1]
Fe_3O_4/FeP	500	50	**10**	30	180	**88%**	This study

To compare the photodegradation effects of TC with different catalysts, Table. 1 categorized several photocatalysts that had been reported in literature[1,6,9,17]. The results showed that Fe_3O_4/FeP-6 contained 88% degradation rates, which was comparable with different reported catalysts , such as FeOOH/FeS_2 of 90%[17], Ag/Fe_3O_4/g-C_3N_4 of 88% [42], $SrTiO_3$/Bi_2O_3 of 85% [9], CDs/MoS_2@H-TiO_2 of 82% [6]. This work is better than Sn_3O_4/g-C_3N_4 of 72% [1].

On the other hand, the dosage (W_{cat}/TC) of Fe_3O_4/FeP-6 was 10 mg/mg, which was the minimum around the rest 5 types of catalysts around 25~50 mg/mg. The amount of catalysts Fe_3O_4/FeP used in photocatalytic experiment was much less with less pollution and lower cost. This is also an advantage of FeP based catalyst as the potential candidate of industrial catalyst in waste water treatment.

3.2 Reusability and stability studies

Reusability and stability are significant factors in evaluating potential applications of photocatalysts.[1] Therefore, Fe_3O_4/FeP-6 were tested by the cyclic degradation experiments under visible light. Fig. 8a-b showed the degradation efficiency of TC over Fe_3O_4/FeP-6 with five runs of cyclic reaction, and it indicated that the degradation rates of TC had a slight decrease (16%) after consecutive photodegradation reaction of five times from 88% to 72%. Results illustrated that the composite Fe_3O_4/FeP-6 had good stability and moderate reusability.

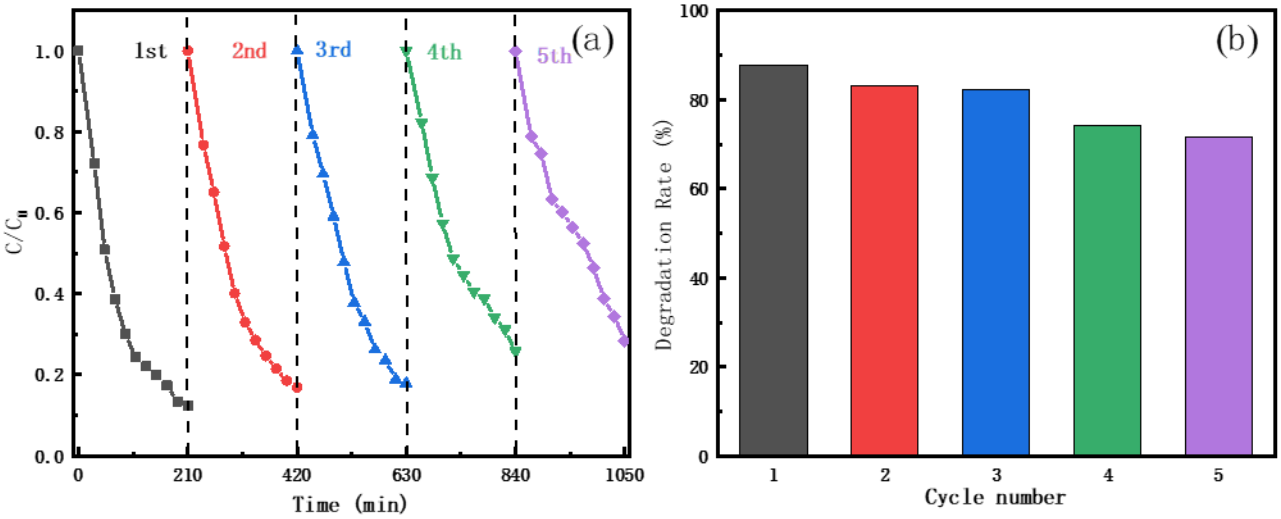

Figure 8. The kinetic curves (a) and photocatalytic degradation rates (b) within five cycle experiments of TC over Fe_3O_4/FeP-6

4. CONCLUSION

A novel photocatalyst of Fe_3O_4/FeP was successfully synthesized through hydrothermal and thermal annealing method. The Fe_3O_4/FeP exhibited superior adsorption performance under dark condition. Based on characterization, the improvement of the adsorption capacity of Fe_3O_4/FeP was ascribed to the special morphology structure along with its large specific surface area. The experimental results showed that Fe_3O_4/FeP-6 (molar ratio of Fe:P is 1:6) had good performance among different ratios in photodegradation effect with 88% removal of TC. This catalyst is comparable to other photocatalysts from reported literature, but with least dose (W/C). Furthermore, the Fe_3O_4/FeP-6 also exhibited good stability and reusability after five cyclic experiments. Results illustrated that Fe_3O_4/FeP

is a potential candidate for TC degradation photocatalyst in the area of pharmaceutical wastewater treatment. The further work may be the improvement of the catalysts to enhance degradation activity.

References

1. C. Li, S. Yu, H. Dong, C. Liu, H. Wu, H. Che, G. Chen, *Appl. Catal., B* 238 (2018) 284.
2. J. Liu, H. Lin, Y. He, Y. Dong, E.Rose, G. Y. Menzembere, *J. Clean Prod.*, 260 (2020).
3. H. Shi, Q. Wu, L. Jang, L. Wang, M. Huang, B. Hang, Z. Yu, Y. Zuo, *Int. J. Electrochem. Sci.*, (2020) 1539.
4. Z. Zhu, Y. Yu, H. Huang, X. Yao, H. Dong, Z. Liu, Y. Yan, C. Li, P. Huo, *Catal. Sci. Technol.*, 7 (2017) 4092.
5. Z. Lu, X. Zhao, Z. Zhu, M. Song, N.L. Gao, Y. Wang, Z. Ma, W. Shi, Y. Yan, H. Dong, *Catal. Sci. Technol.*, 6 (2016) 6513.
6. C. Liu, J. Chen, H. Che, K. Huang, P.A. Charpentier, W. Xu, W.D. Shi, H. Dong, *RSC Adv.*, 7 (2017) 8429.
7. Y. Gao, Y. Li, L. Zhang, H. Huang, J. Hu, S. Shah, X. Su, *J. Colloid Interface Sci.*, 368 (2012) 540.
8. H. Wu, C. Li, H. Che, H. Hu, W. Hu, C. Liu, J. Ai, H. Dong, *Appl. Surf. Sci.*, 440 (2018) 308.
9. H. Che, J. Chen, K. Huang, W. Hu, H. Hu, X. Liu, G. Che, C. Liu, W. Shi, *J. Alloys Compd.*, 688 (2016) 882.
10. L. Liu, L. Ding, Y. Liu, W. An, S. Lin, Y. Liang, W. Cui, *Appl. Catal., B* 201 (2017) 92.
11. D. Selleswari, P. Meena, D. Mangalaraj, *J. Iran. Chem. Soc.*, 16 (2019) 1291.
12. R. Huang, S. Huang, D. Chen, Q. Zhang, T. Le, Q. Wang, Z. Hu, Z. Chen, *J. Colloid Interface Sci.*, 542 (2019) 460.
13. L. Ji, W. Chen, J. Bi, S. Zheng, Z. Xu, D. Zhu, P.J. Alvarez, *Environ. Toxicol. Chem.*, 29 (2010) 2713.
14. R. Daghrir, P. Drogui, D. Robert, *Ind. Eng. Chem. Res.*, 52 (2013) 3581.
15. M. Chong, B. Jin, C.W. Chow, C. Saint, *Water Res.*, 44 (2010) 2997.
16. L. Zhang, C. Niu, C. Liang, X. Wen, D. Huang, H. Guo, X. Zhao, G. Zeng, *Chem. Eng. J.*, 352 (2018) 863.
17. Y. Guo, C. Li, Z. Gong, Y. Guo, X. Wang, B. Gao, W. Qin, G. Wang, *J. Hazard. Mater.*, 397 (2020) 122580.
18. B. Ma, R. Zhang, K. Lin, H. Liu, X. Wang, W. Liu, H. Zhan, *Chin. J. Catal.*, 39 (2018) 527-533.
19. Y. Ni, K. Liao, J. Li, *Cryst. Eng. Comm.*, 12 (2010).
20. S. Liu, L.B. Ma, H. Zhang, C. Ma, *Mater. Sci. Eng., B* 207 (2016) 33.
21. X. Zhang, K. Min, W. Zheng, J. Hwang, B. Han, L.Y.S. Lee, *Appl. Catal., B* 273 (2020).
22. A. Rauf, M. Ma, S. Kim, M.S.A. Sher Shah, C.H. Chung, J.H. Park, P.J. Yoo, *Nanoscale*, 10 (2018) 3026.
23. R. Zhang, P.A. Russo, M. Feist, P. Amsalem, N. Koch, N. Pinna, ACS *Appl. Mater. Interface.*, 9 (2017) 14013.
24. M. Chen, L. Shao, Z. Yuan, Q. Jing, K. Huang, Z. Huang, X. Zhao, G. Zou, *ACS Appl. Mater. Interface.*, 9 (2017) 17949.
25. F. Wang, H. Xue, Z. Tian, W. Xing, L. Feng, *J. Power Sources*, 375 (2018) 37
26. F. Wang, X. Yang, B. Dong, X. Yu, H. Xue, L. Feng, *Electrochem. Commun.*, 92 (2018) 33.
27. D. Xiong, X. Wang, W. Li, L. Liu, *Chem. Commun.*, 52 (2016) 8711.
28. R. Liu, S. Gu, H. Du, C. Li, *J. Mater. Chem. A*, 2 (2014) 17263.
29. C. Ma, S. Feng, J. Zhou, R. Chen, Y. Wei, H. Liu, S. Wang, *Appl. Catal., B* 259 (2019).
30. X. Zhou, B. Jin, R. Chen, F. Peng, Y. Fang, *Mater. Res. Bull.*, 48 (2013) 1447.
31. Z. Lu, W. Zhou, P. Huo, Y. Luo, M. He, J. Pan, C. Li, Y. Yan, *Chem. Eng. J.*, 225 (2013) 34.
32. S. Kumar, S. T, B. Kumar, A. Baruah, V. Shanker, *J. Phys. Chem. C*, 117 (2013) 26135.
33. Y. Ma, C. Hou, H. Zhang, Q. Zhang, H. Liu, S. Wu, Z. Guo, *Electrochim. Acta*, 315 (2019) 114.

34. X. Zhao, Z. Lu, M. Wei, M. Zhang, H. Dong, C. Yi, R. Ji, Y. Yan, *Appl. Catal., B* 220 (2018) 137.
35. J. Huang, Y. Su, Y. Zhang, W. Wu, C. Wu, Y. Sun, R. Lu, G. Zou, Y. Li, J. Xiong, *J. Mater. Chem. A*, 6 (2018) 9467.
36. J. Li, J. Lin, *Mater. Lett.*, 221 (2018) 289.
37. C. Lin, Z. Gao, J. Yang, B. Liu, J. Jin, *J. Mater. Chem. A*, 6 (2018) 6387.
38. J. Guan J, C. Li, J. Zhao, Y. Yang, W. Zhou, Y. Wang, G.R. Li, *Appl. Catal., B* 269 (2020), 269
39. X. Zhang, Y. Liu, S. Dong, Z. Ye, Y. Wei, *J. Alloys Compd.*, 744 (2018) 507.
40. D. Li, Q. Liao, B. Ren, Q. Jin, H. Cui, C.X. Wang, *J. Mater. Chem. A*, 5 (2017) 11301.
41. J. Tian, Q. Liu, Y. Liang, Z. Xing, A.M. Asiri, X. Sun, *ACS Appl. Mater. Interface.*, 6 (2014) 17949.
42. Z. Zhu, Z. Lu, D. Wang, X. Tang, Y.Yan, W. Shi, Y. Wang, N. Gao, X. Yao, H. Dong, *Appl. Catal., B*, 182 (2016) 115.